MICROMACHINED DEVICES AND FABRICATION TECHNOLOGIES

Micromachined (or micromechanical) devices are miniature structures designed for sensing, actuation, and packaging. They are created by micromachining, which constitutes a broad class of fabrication techniques that grew out of the technology and materials of the microelectronics industry. Photolithography, oxidation, diffusion, chemical vapor deposition, evaporation, and wet and dry chemical etching (1) are used not only to create transistors, resistors, and capacitors, but to also create sensors, actuators and packaging structures. By using integrated circuit (IC) processing to create micromachined devices, the integration of electronics with sensors and actuators on a single substrate is possible. Single crystal silicon is the substrate material of choice both because of its dominant use in ICs and because of its superb mechanical and etching characteristics. Applications of micromachining have required the development of augmented and new process technologies to accommodate the unique critical parameters (e.g., stress control) as well as nonstandard materials. The combination of small size and batch fabrication characteristic of IC processing makes micromachined devices particularly applicable for low-cost, high-volume applications. Expanded use of these devices allows more sensors to be incorporated into single or distributed systems and thus allows more widespread use of data collection and electronic control.

Micromachined devices have a minimum feature size in the range of 1 μm to 1 mm. The term "micromachined" seems to imply that the devices are incredibly precise, but this is not the case. While micromachined devices are quite small, they are not created to the same relative tolerance as macroscopic objects made with conventional machining. Objects on the order of a centimeter to a meter can have a relative tolerance of 10^{-4} to 10^{-5}, whereas micromachined devices have a relative tolerance of 10^{-2} to 10^{-3}. So although micromachined devices are small, they are not as accurately fabricated as macroscopic devices.

One of the early commercial applications of a micromachined device was a pressure sensor (2) that appeared in 1962. Diaphragms of silicon were formed by combining wet chemical etching, plasma etching, and oxidation. The piezoresistive effect in silicon was used as the transduction mechanism from the mechanical to electrical domain. Through the 1970s, many companies commercialized other micromachined products such as the Texas Instruments thermal print head (1977) (3), IBM ink jet nozzle arrays (1977) (4) and Hewlett Packard thermally isolated diode detectors (1980) (5). The first commercial application of surface micromachining was the ADXL50 accelerometer from Analog Devices, as shown in Fig. 1 (6). Other materials have also been utilized in micromachined devices such as quartz wristwatch tuning fork resonators (7).

In this article, the fabrication technology of micromachining is presented with the two important techniques, bulk and surface micromachining, being described in detail. In the next section, the fundamental building blocks of micromachined devices are outlined followed by a discussion of the main sensing and actuating physical mechanisms. Finally, some applications of micromachined devices are discussed.

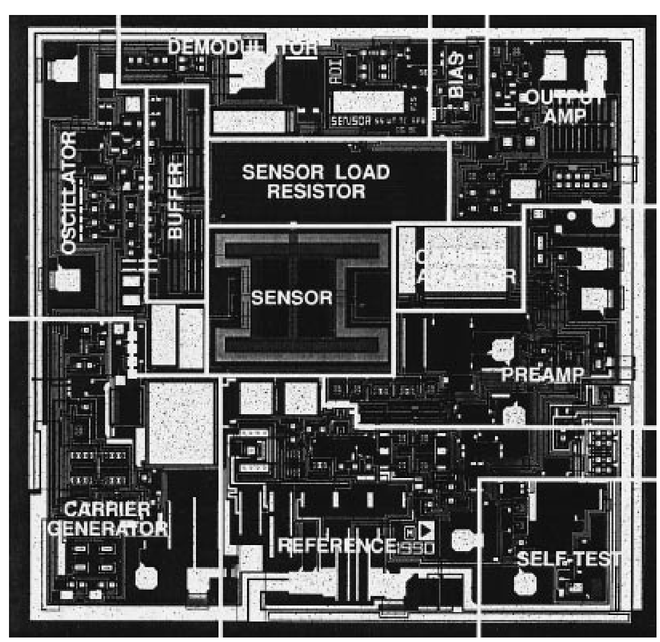

Figure 1. A photomicrograph of the Analog Devices ADXL50, the first surface micromachined accelerometer. (Courtesy of Analog Devices).

BULK MICROMACHINING

Bulk micromachining, which typically refers to any etching of the substrate (isotropically or anisotropically) or bonding of substrates, has been used for over 20 years and remains the most prevalent fabrication process for micromachined devices.

In bulk micromachining, the silicon substrate itself is machined to form a functional component in a sensor, actuator, or package. Bulk micromachined structures include diaphragms, membranes, cantilever beams, V-grooves, and through-wafer holes that are created primarily with anisotropic etching of the substrate. The anisotropic etch produces tight dimensional control even in structures that are as thick as the substrate. By selecting different crystal orientations for the initial substrate, different etch profiles can be produced (see Wolf (1) for a description of crystals and crystal notation). For example, a ⟨110⟩ wafer will produce vertical sidewalls when etched in an anisotropic etchant. Thin films can be deposited on the substrate surface to create transducing layers (i.e., piezoresistive or piezoelectric films), etch stop layers, or isolation layers. Two-sided processing is common and has the benefit of separating the electronics from the sensing environment, thus allowing the sensors to be used in hazardous environments. More complicated structures, such as accelerometers, gyros, valves, and pumps, can be created by incorporating wafer bonding techniques.

Materials

The most commonly used substrate for bulk micromachining is single-crystal silicon. Silicon has a diamond-cubic atomic structure (1). The crystalline structure lends itself well to anisotropic etching along the crystal planes. By changing the orientation of the substrate to the crystal planes, different resulting etch profiles can be created. Silicon wafers are also abundant and inexpensive. Because of the single crystal nature and purity of silicon wafers, the mechanical properties are well controlled (8). Silicon is stronger than steel, but is also very brittle. The elastic behavior of silicon makes the fabrication of reliable and repeatable structures possible. Many sensors can be created from silicon because it is sensitive to stress, temperature, radiation, and magnetic fields as discussed in the sections below.

Silicon dioxide (glass) substrates are also commonly used, especially in bonding with other substrates. The mechanical characteristics and melting points of glass can be modified by changing the level of doping impurities in the glass. The addition of sodium creates substrates that work well with anodic bonding. Corning #7750 glass is best suited for bonding to ⟨100⟩ silicon substrates because the coefficient of thermal expansion is matched to that of silicon. The melting point of doped glass puts an upper limit on the temperature that can be used in subsequent processing and on the operating temperature of the device.

Quartz is the single-crystal form of silicon dioxide. Like silicon, quartz can be anisotropically etched (9). The most important characteristic of quartz is that it has a large piezoelectric effect (see below). Quartz, however, is quite fragile and must be handled with care. As with silicon, the crystal orientations of the quartz produce different mechanical and electrical characteristics. Table 1 shows some of the mechanical parameters of both single-crystal silicon and quartz. Other substrates such as gallium arsenide have been utilized for micromachining, but their high cost has limited their applications.

Table 1. Mechanical Properties of Bulk Silicon and Quartz

Property	Silicon	Quartz
Young's modulus (GPa)	129.5×10^9 [100]	
	168.0×10^9 [110]	
	186.5×10^9 [111]	
Yield strength	7 GPa	
Coefficient of thermal expansion (°C^{-1})	2.33×10^{-6}	$7.1 \times 10^{-6} \parallel Z$
		$13.2 \times 10^{-6} \perp Z$
Thermal conductivity (W/mK) at 300°C	15.7	$29 \parallel Z$
		$16 \perp Z$
Density (kg/m^3)	2300	2660
Melting point	1350°C	1710°C

Wet Anisotropic Silicon Etching

Wet anisotropic etchants create three-dimensional structures in a crystalline silicon substrate because the etch rate depends on the crystal orientation. Typically, the etch rate is fastest along the ⟨100⟩ and ⟨110⟩ directions and slowest along the ⟨111⟩ directions. Since silicon dioxide (SiO_2)and silicon nitride (Si_3N_4) are etched more slowly than silicon, they can be used as masking films or etch stops. Some silicon etchants also have a reduced etch rate in the presence of heavy boron doping, thus allowing a boron-doped layer to act as an etch stop in silicon.

A tremendous variety of structures can be created using combinations of silicon dioxide, silicon nitride, and boron diffused etch stops, front- and back-side lithography, and silicon substrates with different crystal orientations. For a ⟨100⟩ silicon substrate the mask is aligned to the [110] direction. This will create an etched feature that terminates at the mask edge. Figure 2 shows the progress of the etch of three different types of simple structures in ⟨100⟩ silicon: a V-groove, a diaphragm, and a through-wafer hole. As the etch proceeds {111} planes form along the edges of the silicon nitride etch masks. These planes form a 54.7° angle with the (100) surface of the wafer. If allowed, the etch will continue until only {111} planes are exposed. The angle between the {100} and {111} planes causes the size of the etch pit for the diaphragm and through hole to be much larger than the whole opening. This drawback can be compensated for by using a bonded wafer for the membrane. If the substrate is not aligned well to the [110] direction, the etched feature will underetch the mask until only the {111} planes are visible. Figure 3 illustrates the resulting structure due to a mask misalignment. Some applications require vertical sidewalls in the silicon substrate. This is accomplished with ⟨110⟩ substrates. The alignment of the mask is to the [111] direction. The {111} planes are perpendicular to the wafer surface. The etch proceeds as before, etching all planes except the {111} planes. It is thus easy to create through wafer slits with ⟨110⟩ substrates. For a more detailed review of bulk micromachining, see Ref. (10).

High etch selectivities between different crystal orientations and masking materials allows lateral as well as vertical dimensions to be controlled to within 0.5 μm or better. However, while the dimensions of the structures are accurate, there are some problems with wet anisotropic etching of sili-

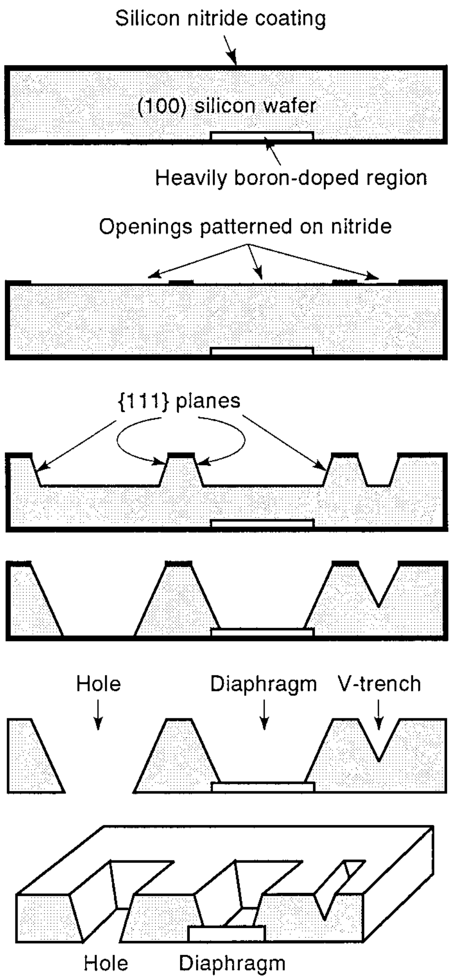

Figure 2. The progress of the etch of three different types of simple structures in ⟨100⟩ silicon: a V-groove, a diaphragm, and a through-wafer hole. Note the use of the boron-diffused silicon membrane. (After Ref. 10.)

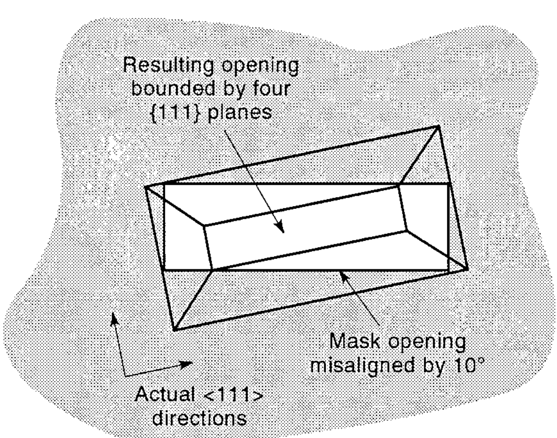

Figure 3. Effect of misalignment between the mask and the actual ⟨111⟩ directions on the final etch profile. Note that the etched feature always increases in size due to misalignment. Also, that the etch feature is bounded by {111} planes.

con. All of the chemistries etch silicon at ≈1 μm/min in the fast etching orientation, ⟨100⟩. Thus, to etch through an entire 500 μm wafer over 8 hours are required. In addition, the etch rates and performance depends on temperature and concentration of the solutions. The three main wet anisotropic silicon etchants and their characteristics are listed in Table 2. Finally, although the anisotropically etched structures are three-dimensional, there are only a few types of vertical features that can be created (i.e., vertical and angled at 54.7°).

The most common anisotropic etchant is a mixture of potassium hydroxide (KOH), water, and isopropyl alcohol at 80°C (11,12). At higher temperatures the uniformity of the etch decreases. The concentration of KOH can be varied from 10 wt% to 50 wt% (2 M to 12 M). High KOH concentrations result in smooth structures. Hydrogen gas is generated as a byproduct of the etch and forms bubbles which are thought to cause the surface roughness seen at low KOH concentrations. The main advantage of KOH is that it has the highest etch rate ratio between the {100} and {111} planes, 400 to 600. On the other hand, KOH is not compatible with IC fabrication because of the presence of the mobile ion, K^+. KOH also etches silicon dioxide at ≈28 Å/min, which makes oxide unusable as a masking material for through-wafer etches. Silicon nitride, which is not attacked, must be used as the masking material in long KOH etches.

Another common anisotropic etchant is a mixture of ethylenediamine/pyrocatechol (EDP) and water at 115°C (13). This etchant is a thick, opaque liquid that ages quickly when exposed to oxygen. A reflux system is required to keep the composition of the solution constant as well as provide a nitrogen atmosphere to prevent aging. When mixing this etchant the water is added last because the water triggers the oxygen sensitivity. The main advantage of EDP is that it etches oxide much more slowly than KOH. The oxide to (100) silicon etch rate ratio is 5000 for EDP and 400 for KOH. Also, EDP is more selective to boron doped masking than KOH. Care must be taken when mixing the solution because EDP is toxic.

Tetramethyl ammonium hydroxide (TMAH) (14) is of interest because it is more stable than EDP, has a high selectivity of oxide to silicon, and is compatible with complementary metal-oxide-semiconductor (CMOS) circuit fabrication. This makes TMAH useful for high-volume production applications. However, the etch rate ratio of (100)/(111) silicon is only 12.5 to 50. Many other alkaline solutions have been studied: hydrazine, sodium hydroxide, ammonium hydroxide, cesium hydroxide, and tetraethyl ammonium hydroxide.

Dry Anisotropic Silicon Etching

An area of active research is high aspect ratio microstructures (HARM). Either bulk silicon, silicon on insulator, or thick (i.e., >10 μm) polysilicon is etched anisotropically to form structures that have a thickness-to-width ratio as high as 100. Whereas anisotropic etching of ⟨110⟩ silicon can form tall, narrow structures, plasma etching is easier to use. The plasma etch is performed by alternating between a silicon etch (e.g., Cl_2 or SF_6) and a plasma polymerization step based on a fluorocarbon. One drawback of this etch is the 1 μm/min to 2 μm/min etch rate. Thus for a 650 μm thick silicon wafer it would take approximately 5 h to etch through the wafer. Much research is being carried out to increase the etch rate,

Table 2. Common Wet Anisotropic Silicon Etchants and Characteristics (10)

Etchant	Etch Rate (100) μm/min	Etch Rate Ratio (100)/(111)	Masking Materials	Boron Etch Stops
KOH/water, isopropyl alcohol, 85°C	1.25	400	Si_3N_4 (not etched), SiO_2 (28 A/min)	B > 10^{20} cm^{-3} reduces *e*/*r* by 20
EDP/wafer., pyrazine, 115°C	1.25	35	Si_3N_4 (2–5 A/min), SiO_2 (1 A/min), many metals	B > 5 × 10^{19} cm^{-3} reduces *e*/*r* by 50
TMAH/wafer, 90°C	1.0	1.25–50	Si_3N_4, SiO_2 (1 A/min), many metals	B > 4 × 10^{20} cm^{-3} reduces *e*/*r* by 40

but a value of 10 μm/min is probably the limit for the near future.

An interesting application of this technology uses the anisotropic plasma etch to form a mold in which a thin sacrificial oxide layer is deposited followed by a polysilicon thin film (termed Hexil) (15). The oxide is then removed with hydrofluoric acid (HF) as in surface micromachining, and the resulting polysilicon structure is detached from the substrate. This allows the creation of structures with milliscale dimensions (50 μm to 100 μm tall) using 2 μm films.

Wafer Bonding

In wafer bonding processes, two substrates are bonded together either with an intermediate layer to promote adhesion or directly together without an intermediate layer. Pressure and heat are applied to the two or more substrates during the bonding process. Higher-temperature processing typically results in bonds with higher levels of hermiticity and strength. Anodic bonding, fusion bonding, low-temperature glass bonding, and reactive metal sealing are common techniques for wafer bonding. For all bonding techniques, alignment of the substrates is accomplished either by two-sided alignment or by infrared alignment. The quality of the bond can be ascertained by looking at the wafers in visible wavelengths if transparent substrates are used, or in infrared (IR) wavelengths if silicon substrates are used.

Anodic bonding, also known as electrostatic bonding (16) or field-assisted thermal bonding, is used to bond silicon and sodium-rich glass substrates. A commonly used glass is Corning #7740 (Pyrex) because it has a thermal expansion coefficient that is matched to silicon. This helps to prevent failure of the bond due to residual thermal stresses. The anodic bonding process can take place in air or vacuum (Fig. 4). The silicon and glass wafer are brought in contact and placed on a hot plate at a relatively low temperature, 350° to 450°C. An electrostatic potential of 400 V to 700 V is then applied between the substrates using the glass substrate as the anode. The mobile sodium ions are thus depleted from the interface. This creates a depletion region of about 1 μm with high electric fields of 4–7 × 10^6 V/m. An electrostatic pressure is thus induced between the substrates and is the driving force for the bond (17).

Fusion bonding (18) is the fusing of two wafers thermally without the need for a intermediate adhesion layer. The wafers must be cleaned and placed in contact. The wafers will initially stick together because of van der Waals forces. A force is then applied to the stack of wafers and the assembly is annealed at high temperatures. The resulting bond is very strong and hermetic, but the high temperatures preclude the use of integrated electronics on the wafers. Also, the flatness and cleanliness of the wafers are critical in producing a quality bond.

Both anodic and fusion bonding are not compatible with electronics. To bond in the presence of electronic circuits,

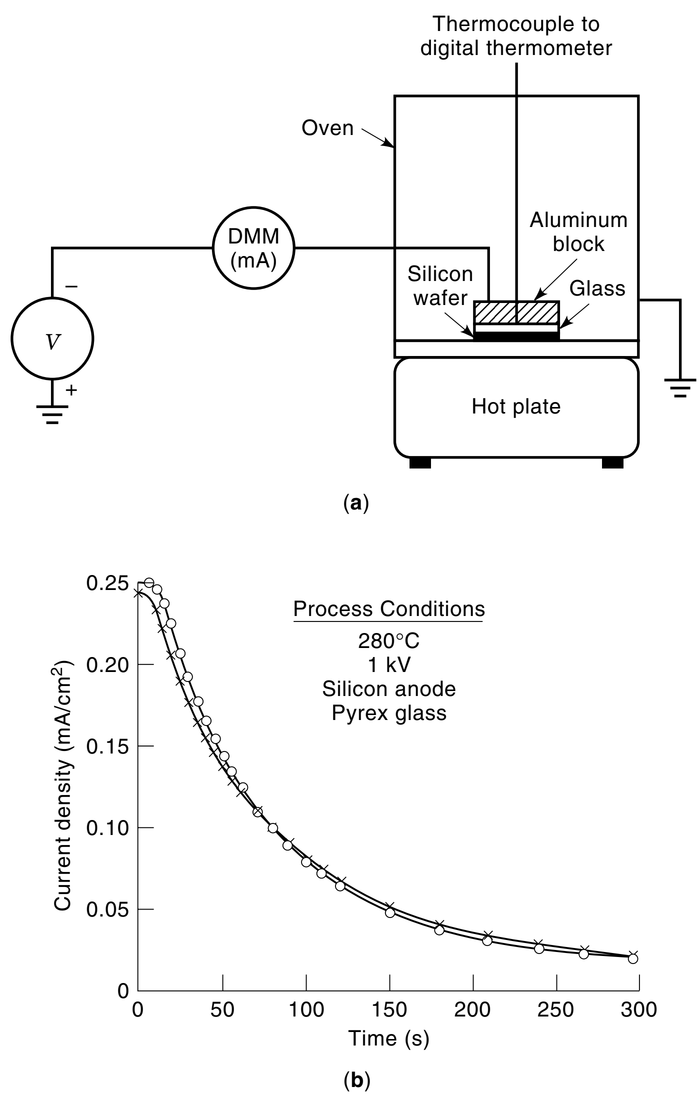

Figure 4. (a) Diagram of the anodic bonding apparatus. When the electric field is applied, the wafer assembly is pressed together and the bond is formed. (b) Plot of typical current through the wafer assembly versus time. When the current falls to 10% of the initial value, the bond is complete. (After Ref. 87.)

techniques which use an intermediate bonding layer are required. This adhesive layer can be low-temperature glass, reactive metal, or organic films (19). All these bonds occur at low temperatures, but each have different thermal characteristics and can thus generate thermal stresses. Also, none of these bonds are hermetic and all require flat wafers to ensure quality bonds.

Isotropic Silicon Etches

Xenon difluoride (XeF_2), when exposed to silicon at a reduced pressure (2 torr), will selectively etch silicon at several hundred micrometers per minute. The selectivities of XeF_2 to oxides, nitrides, and metals are 100 : 1, 100 : 1, and 200 : 1, respectively. XeF_2 has been used to integrate standard circuit processes with microstructures such as accelerometers (20). Typical structures are created as composites of metal and polysilicon encased in silicon dioxide or silicon nitride. The substrate under these structures is isotropically removed to create freestanding structures. Although this approach is very inexpensive, it suffers because the structure is made from a composite of oxide, polysilicon, and metals and is less reliable than silicon or polysilicon alone. Also, the isotropic nature of the etch creates a large undercut around the perimeter of the etch hole. Silicon can also be etched in mixtures of nitric acid (HNO_3) and hydrofluoric acid (HF) (21), but the selectivities are much worse than those for XeF_2.

SURFACE MICROMACHINING

In surface micromachining, devices are created from thin films that are deposited and patterned on the surface of much thicker substrates. The underlying layers are then selectively removed, thus creating a free-standing structure which is attached to the substrate. Many layers can be used to sequentially build up complicated structures such as gears and motors (22) (see Fig. 5 for an example). The thin films are typically 0.1 μm to 10 μm thick, as compared to the substrate, which is 500 μm to 700 μm thick. The resulting devices are comprised of many stacked thin films, but are still essentially two-dimensional (2-D) planar structures. This is in contrast to bulk micromachining, which shapes the substrate to create a more truly three-dimensional (3-D) structure.

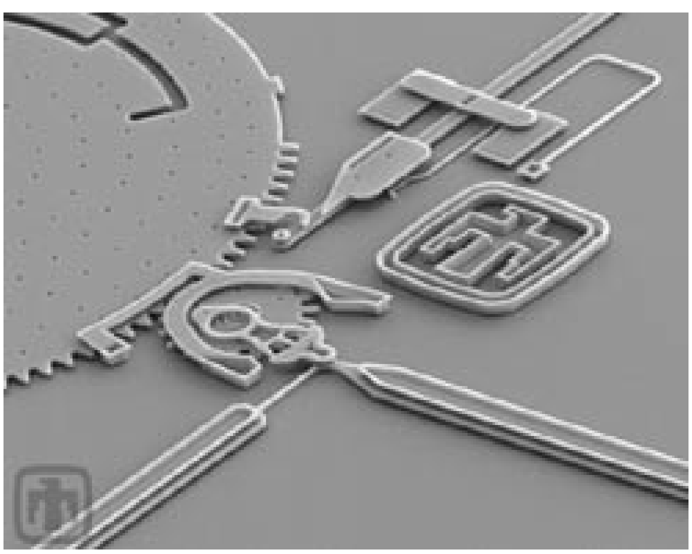

Figure 5. A scanning electron micrograph of a complex surface micromachined mechanism. The mechanism in the center converts the linear motion of the long beam on the right to a rotary motion of the small gear. Note that two different structural polysilicon layers are used. (Courtesy of Sandia National Labs.)

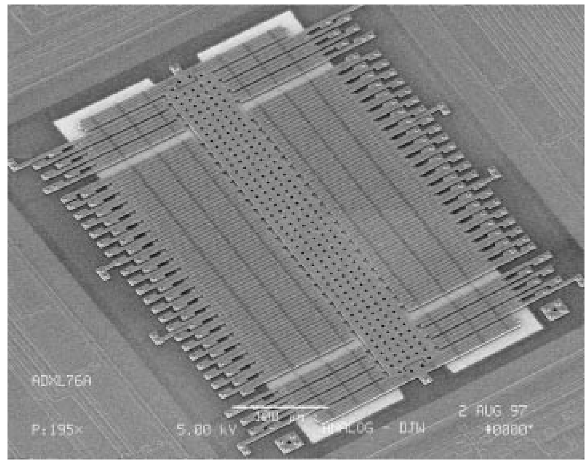

Figure 6. A scanning electron micrograph of the Analog Devices ADXL76, an integrated, micromachined accelerometer. The sensor is fabricated from a 2 μm thick polysilicon structure and is ~500 μm along the long axis. (Courtesy of Analog Devices.)

Surface micromachining was first demonstrated in 1965. An electromechanical filter was created using a gold cantilever as the free-standing gate of a field-effect transistor (23). Only input signals near one-half the resonant frequency of the cantilever would create any output of the field effect transistor. In 1984, the first polycrystalline silicon surface micromachined devices were fabricated (24). By the early 1990s, the first integrated surface micromachined process was developed by Analog Devices (25). Figure 6 shows the ADXL76 structure, a ± 50 g full-scale integrated lateral accelerometer created from a 2 μm thick polysilicon layer. Also, in the 1980s, the digital micromirror device (DMD) was created using aluminum as the mechanical structure (26).

The most basic surface micromachining process produces a single structural layer suspended over the substrate. Figure 7 outlines the process for polysilicon surface micromachining. The process begins with the deposition and patterning of a silicon dioxide to form anchor points for the micromechanical films. The oxide acts as a sacrificial film that will be removed later in the process. Next, polysilicon is deposited and patterned. Polysilicon is the structural micromechanical film out of which the micromachined device will be created. The lateral dimensions are defined by photolithography and etching while the vertical dimensions are defined by film thickness. The final step is the selective removal of the underlying film using a selective chemical etch (i.e., hydrofluoric acid, HF) and the drying of the devices. Preventing the structures from sticking to the substrate or to each other during drying has been the subject of much research. Drying techniques such as supercritical point drying (27) or sublimation (28) have been used to eliminate the surface tension forces. In addition, special anti-stick coatings like Teflon and self-assembling molecules (SAMs) have been deposited after the removal of the sacrificial oxide (29).

One of the major advantages of surface micromachining is the possible economical integration of electronics with the sensor. Surface micromachining produces structures that have smaller dimensions than those fabricated by bulk techniques and thus have smaller signals to external stimulus. The integration of the electronics can make up for this small signal because it reduces the parasitic losses between the sensor and the electronics.

Materials

Any thin film can be used in surface micromachining, although chemical vapor deposition (CVD) films offer the best repeatability. The key is finding suitable pairs of materials where an etchant exists that will selectively remove the lower layer and thus create a free-standing micromachined structure. The most prevalent CVD films are silicon dioxide, silicon nitride, and polycrystalline or amorphous silicon. These films are most commonly deposited using low-pressure chemical vapor deposition (LPCVD). Other thin films that have been used include polyimides, electroplated or deposited metals (aluminum, nickel, tungsten, and nickel-iron), and polymers. The mechanical characteristics of the thin films differ from the corresponding bulk materials because surface effects begin to dominate. Also, the assumption that the grain size is small relative to the dimensions of the devices is no longer valid, and statistical variations in the mechanical parameters like Young's modulus become significant. Finally, in thin films both the axial stress and the stress gradient through the thickness of the film are critical. Compressive stresses can cause buckling of constrained mechanical structures. Excessive stress gradients can cause the films to curl up off of the substrate.

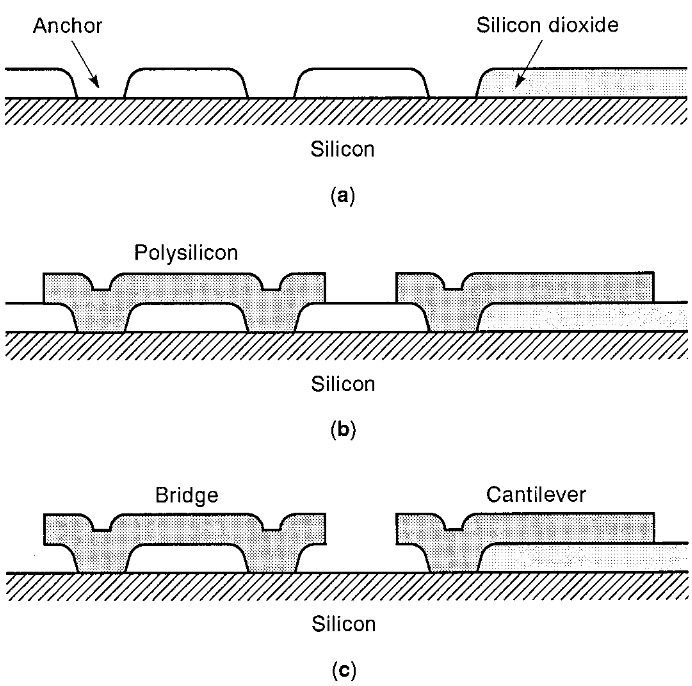

Figure 7. Illustration of surface micromachining—a cantilever–bridge example. (a) Deposit and pattern the sacrificial oxide film; (b) deposit and pattern the structural film (e.g., polysilicon); (c) selectively remove the underlying sacrificial film to create a free-standing micromechanical element. Note that the thickness of the structure is defined by the deposition thickness and that the in-plane dimensions are defined by photolithography and etching.

Polysilicon has similar material characteristics as single-crystal silicon and is therefore a desirable mechanical material. However, the material parameters of polysilicon change with different deposition, doping, and annealing conditions. For example, Young's modulus and yield stress vary somewhat due to processing, but the amount of variation is small compared with that of residual stress and stress gradient. Extensive studies have explored polysilicon including original work by Guckel (30) and Howe (31) and subsequent investigations of *in situ* doping (32), fine-grained polysilicon (33), and correlations between texture and stress and stress gradient (34).

Integration

Integration of electronics with surface micromachined devices is intrinsically simpler because only one side of the wafer is utilized. In addition, the wafers are not as fragile, at least not until the surface micromachined structures are released from the substrate. There are three approaches to integration of microstructures: precircuit, mixed, and postcircuit processing. Almost all integrated technologies involve some level of mixing between the circuit and micromechanical processing steps. It is thus by the division of the majority of the processing steps that the techniques are characterized. By fabricating the micromachined devices prior to the circuit processing, the high-temperature anneals which are required to relieve the stresses in the thin films will not detrimentally affect the circuit processing. Similarly, the circuit processing must also not effect the microstructures, which is typical as the circuit processes use lower temperatures. The topography of the surface micromachined devices requires planarization. Sandia National Labs has demonstrated a "structures-first" process using CMOS electronics (35). Unless the structures are released from the substrate and encapsulated, the structures will need to be released from the substrate after the circuit processing is complete.

A mixed integration strategy, like that used by Analog Devices (25), further interweaves the circuit and microstructure processing. For example, the high-temperature circuit processing would be completed first, followed by the microstructure fabrication, then the rest of the circuit processing. Polysilicon/silicon dioxide surface micromachining is an example of a technique that works well with preintegration or mixed integration. The high-temperature anneals and topology issues are minimized by gradually building up the structures and choosing the timing of the anneals to minimize their impacts on the already created devices.

Integrating the microstructures after the circuit processing is the closest to a modular technique. After the metal is etched and passivated, the microstructures are fabricated. The presence of the metal precludes the use of high-temperature anneals unless special metalization like tungsten is used (36). Electroplating techniques or deposited metal/polymer surface micromachining allows the use of conventional circuits, but the mechanical characteristics of the metal structures are not as desirable as polysilicon. As described above, XeF_2 can be used to selectively remove the silicon substrate to release a composite microstructure of oxide, polysilicon, and metal. The mechanical characteristics of this composite structure are also not as desirable as those of polysilicon, but the simplicity of the process makes some low-cost applications very attractive.

Other Micromachining Technologies

Although surface and bulk micromachining can be used to create a large variety of structures, there are applications and materials that require other micromachining technologies. For example, many applications require truly 3-D structures such as the miniaturization of mechanical systems (e.g., clocks) and microrobotics. In general, surface micromachining is limited to structures in the plane of the substrate. The in-plane dimensions are controlled by lithography and thus have great design freedom, but the thickness is controlled by a deposition thickness and is thus fixed. Bulk micromachining, on the other hand, does create 3-D structures, but the shapes are constrained by the crystallographic planes.

Surface micromachining has created hinged polysilicon structures (37) that can be erected above the substrate, but the thickness of each element is still limited to the thickness of the deposition. An active area of research is high-aspect ratio structures. These thick planar structures can be created with electroplating or highly anisotropic silicon etches. Although these structures are still planar, the additional thickness produces structures with more mass and additional robustness. Many other technologies exist including electron discharge machining (38), focused ion-beam milling (39), ultrasonic machining (40), laser-assisted etching and deposition, 3-D photolithography, and ultrahigh-precision mechanical machining.

LIGA. The German Lithographie Galvanoformung Abformtechnik (LIGA) is a technique that consists of lithography, electroplating, and molding (41). The lithography process uses a 100 μm to 500 μm thick layer of photoresist [e.g., polymethylmethacrylate (PMMA)] on a conductive substrate. High-energy synchrotron X-ray radiation is used to expose the photoresist. A special X-ray mask is required that uses gold to absorb the X-ray radiation. After development, the desired thick, high-aspect-ratio resist structure is obtained. Metal is subsequently electroplated on the conductive substrate. After resist removal, a free-standing metal structure is obtained. This structure can be used as the final product or as an injection mold for plastic parts. The injection mold can be reused and is thus an inexpensive way of creating precision plastic parts, although the fabrication of the mold itself is expensive.

Although LIGA produces relatively thick microstructures, they are 2-D. To create more complex, multilevel devices, structures produces by the basic process will require assembly (42). There have been many modifications to LIGA that include placing a patterned sacrificial film such as silicon dioxide, photoresist, or polysilicon under the metal LIGA structures to create a free-standing structure (43). In addition, multiple layers of LIGA are now possible by repeating the basic process with a planarization process between the two LIGA processes. Applications such as electromagnetic micromotors (44) and an electromagnetic dynamometer (45) have been produced using LIGA.

MICROMACHINED DEVICES AND APPLICATIONS

The purpose of this section is twofold: (1) to examine quantitatively some of the fundamental building blocks (or models) used in typical micromachined device design and (2) to examine several broad classes of micromachined devices to give the reader a feeling for the possible application areas to which micromachined devices can be applied. We will start with the building blocks because they form the physical underpinning of the functional mechanisms of actual micromachined devices.

The Building Blocks of Micromachined Devices

Since almost any structure built using the broad class of MEMS fabrication techniques can be considered a micromachined device, it is rather presumptuous to make a list of building blocks for MEMS. However, as micromachined devices have evolved, a group of canonical structures have become ubiquitous. These structures, and the simple models used for their first-cut design, form the basis for the design of many micromachined systems.

The Diaphragm. Arguably, the most basic micromachined structure is the thin-film diaphragm. The fundamental function of a diaphragm in a micromachined device is to deform under a load. This deformation is then sensed, typically with either (1) piezoresistors, which sense changes in stress, or (2) a capacitance measurement that is sensitive to changes in the deflection itself. Figure 8 is a sketch of a diaphragm cross section with an embedded (diffused) piezoresistor. The fundamental design relationship for a thin diaphragm is the deflection versus applied load relation (9):

$$\frac{\partial^4 w}{\partial x^4} + \frac{\partial^4 w}{\partial x^2\, dy^2} + \frac{\partial^4 w}{\partial y^4} = \frac{12(1-\nu^2)p}{Et^3} \tag{1}$$

where w is the z-axis deflection as a function of the x and y position, p is a uniform applied pressure load, t is the diaphragm thickness, ν is Poisson's ratio, and E is Young's modulus (or the modulus of elasticity). Equation (1) must be solved in conjunction with the appropriate boundary conditions for the case under study (for example, the diaphragm is fixed along its entire edge). In general, such solutions are best performed by numerical methods such as finite element analysis (FEA) (46), especially in cases where residual stress effects must be added to Eq. (1). However, approximate design relations have been developed (47). For a square membrane, the maximum absolute value of the stress occurs at the center

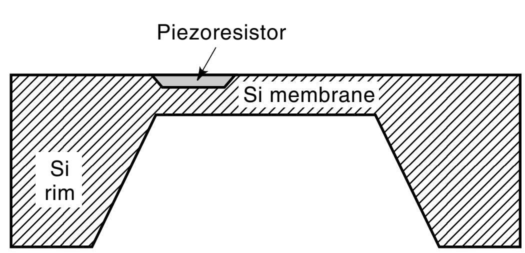

Figure 8. Cross-sectional sketch of a micromachined diaphragm with a diffused piezoresistor. Note that the thickness of the diaphragm is not to scale. (After Ref. 10.)

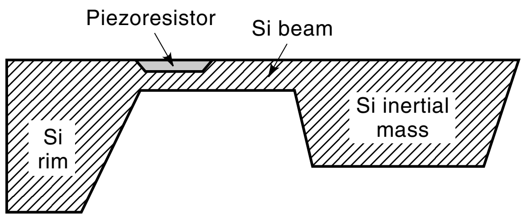

Figure 9. Cross-sectional sketch of a micromachined accelerometer with piezoresistive sensing. The device is made up of a bulk micromachined silicon beam with an inertial ("proof") mass attached to its free end. Note that the beam width (into the page) is typically much thinner than the proof mass. Often there are multiple beams supporting one proof mass. (After Ref. 10.)

of the sides of the membrane and decreases toward the corners and the center of the membrane. The surface stress in the middle of a side can be approximated as

$$\sigma_{\max} \approx 0.31p\,\frac{a^2}{t^2} \tag{2}$$

where a is the membrane side length. Note that the maximum stress magnitude is proportional to the square of the side length-to-thickness ratio. This ratio is constrained by sensor area constraints and the strength and manufacturability of the thin membrane.

Beams and the Spring-Mass System. We saw that the fundamental relationship for the diaphragm was the force displacement relation. Beams behave in a similar manner. The deflection characteristics of beams under various loading conditions and various boundary constraints have been tabulated (48).

Beams have an even more powerful building-block function in the context of lumped tether-plate (spring-mass) systems. The typical arrangement contains a plate, which constitutes the mass, and a set of beams (tethers) which form the spring. Figure 9 shows a cross-sectional sketch of a cantilever beam which is fixed to the silicon substrate (rim) on one side and has an attached inertial ("proof") mass on the other. Modeling this type of structure as a lumped spring-mass system assumes that the plate mass moves as a rigid body and all of the bending occurs in the beams (tethers). In addition to a simple force versus displacement relation, such systems are resonant, with the resonant frequency given by

$$f_{\mathrm{r}} = \frac{1}{2\pi}\sqrt{\frac{k}{M}} \tag{3}$$

where k is the spring constant and M is the mass of the system. In the case where the beams can be treated as idealized linear lumped elements, the spring constant can be found:

$$k = \frac{3EI}{L^3} \tag{4}$$

where I is the area moment of inertia around the centroidal axis of the beam cross-section, and L is the beam length. More complex spring structures can be created by combining these simple cantilever elements in series or parallel. This relationship ignores the effect of residual stress in the beam and is valid for small displacements. Residual stresses will exist for any structure with more than one anchor point. To build structures which do not suffer from the complication of significant residual stress effects, micromachined tethers are often built as folded tethers, as shown in Fig. 10. Such structures have the benefit of being compact; but even more important, any residual or built-in stresses in the beams are allowed to relax. The spring constant of a folded tether (such as one of the four tethers in Fig. 10) can be approximated as two long beams in series. Clearly, a parallel set of relations can be developed for a beam in torsion yielding a torsional spring, moment of inertia system.

Capacitive Elements. A fundamental element for both sensing and actuation is the air-gap capacitor. Such a capacitor consists of a pair of conductors separated by a gap that allows one or both of the conductors to move. If the conductor is moved due to an applied force, the capacitance between the conductors changes. This change in capacitance can be measured electrically. Given an applied voltage, the same capacitance structure yields a force, which can be exploited for actuation.

The canonical capacitance structure is the parallel-plate capacitor. Such structures are often made up of a conductive surface on a bulk micromachined structure (e.g., a diaphragm) and a counterelectrode on an adjacent wafer-bonded surface. In surface micromachining, one capacitor plate is often made from the suspended structural film and the other plate is a conducting electrode on the substrate surface. For cases where the lateral extent of the capacitor is large compared to the gap between the electrodes (i.e., fringing fields can be neglected), the relation for the capacitance of an infinite parallel plate capacitor is an appropriate model:

$$C_{\mathrm{pp}} = \frac{\epsilon A}{g} \tag{5}$$

where A is the area of the capacitor, g is the gap between the capacitor plates, and ϵ is the permittivity of the material in the capacitor gap.

The other canonical microfabricated capacitance structure occurs in cases where the motion to be sensed or actuated is in the plane of the thin film. This leads to the interdigitated

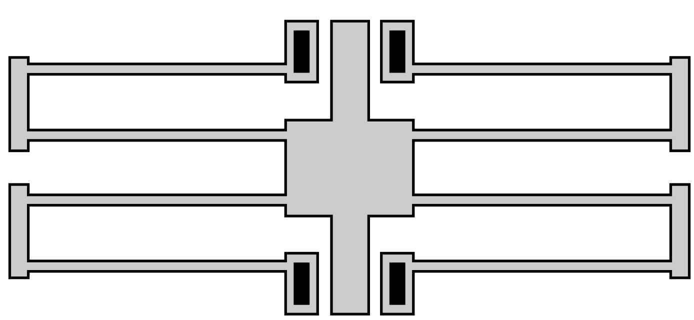

Figure 10. Sketch of a spring-mass system where the four springs are beam structures known as a folded flexures. These compact spring structures have the additional advantage that they allow residual stresses to relax. Thus their stiffness is not a function of residual stress.

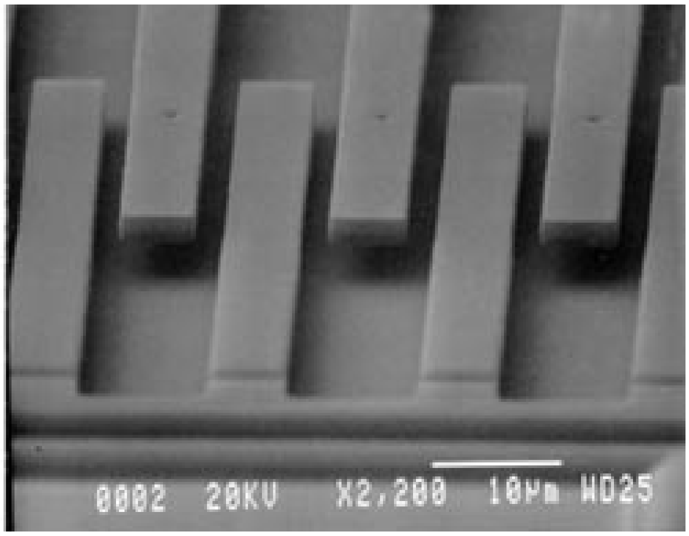

Figure 11. A scanning electron micrograph of a typical surface micromachined interdigitated finger array. (Courtesy of MCNC.)

finger structure as shown in Fig. 11. Calculation of the capacitance in this case is more difficult because the aspect ratio of the gap to the characteristic electrode dimension is close to 1. Consequently, the electric field has a large fringing field component and the parallel plate capacitance approximation is no longer valid. In general, 3-D numerical computations are required to obtain accurate values in this case (46). It is possible to use a correction factor in Eq. (5) to get a reasonably accurate closed-form solution for small perturbations to the geometry. However, these correction factors must, in general, be computed numerically, and their accuracy is generally limited to small displacements.

Pivots and Bearings. In addition to constrained, spring-mass type motions, structures have been fabricated that allow untethered motions. Constructions which allow free rotations are typically planar pin joints (22) or out-of-plane hinges (37). Hinges can be fabricated by using two polysilicon layers, with one layer as the stationary hinge and one layer as the rotating part. Figure 12 shows a close-up scanning electron micrograph of an out-of-plane hinge joint. Figure 13 shows an example of a pin bearing in the form of a variable capacitance micromachined motor. In addition, linear sliding constraints have been constructed (22). Further increasing the number of polysilicon layers allows the creation of ever more complicated joints and bearings. One application of hinges is in microptical systems such as bar code readers (49).

Isolated Thermal Mass. The most basic structure in micromachined thermal sensors is the thermally isolated (or "floating") thermal mass. Micromachining allows masses to be built with mechanical supports which have very small cross sections and thus very small thermal conductivities. Such isolation allows physical transduction to occur without significant thermal influence from the surrounding support wafer. The use of a metal film or a diffused conductive "wire" allows heaters and thermal sensors to be placed on these floating thermal masses.

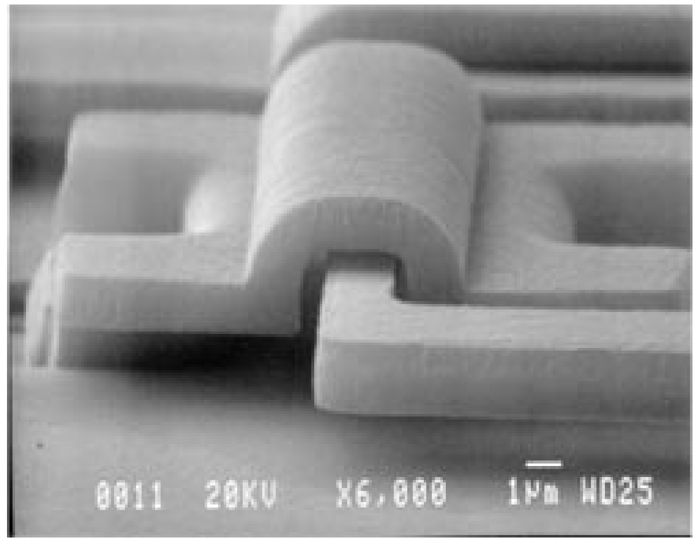

Figure 12. A scanning electron micrograph of a surface micromachined hinge joint. The movable portion (U-shaped part from center to right) is made from the first polysilicon layer. The fixed hinge (jumps up and over the central beam) is made from the second polysilicon layer. The depressed areas to the left and right of the fixed hinge are the anchor areas that fix the hinge to the substrate. (Courtesy of MCNC.)

Sensing and Actuation Mechanisms

A sensing mechanism is any physical effect that converts energy from one form to another. In most practical sensors (or actuators), conversion into (or from) an electrical signal is the desired goal. There are many, many physical transduction mechanisms, which might be exploited for sensors or actuators. Here we will examine several that are widely used in

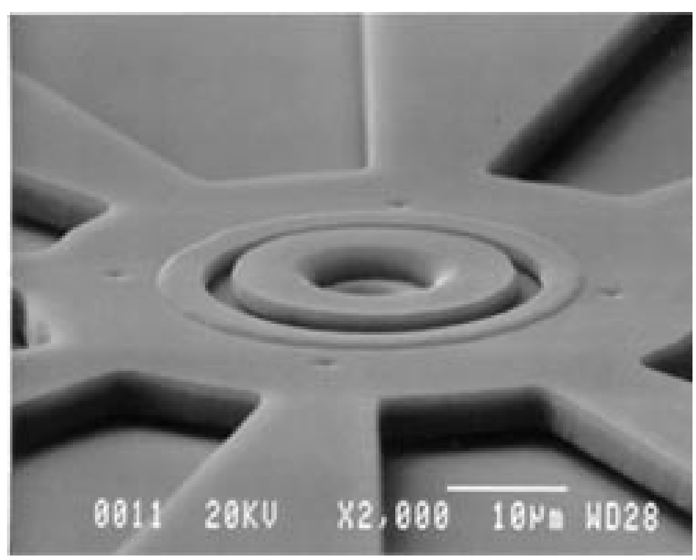

Figure 13. A scanning electron micrograph of a typical surface micromachined rotary pin bearing. The mushroom-shaped structure in the center is the pin, which is fixed to the substrate by the anchor in the very center. The central section of the rotor is under the cap of the pin and thus is constrained to rotary motions around the pin. (Courtesy of MCNC.)

MEMS. Other mechanisms include floating gate transistor devices (23), electron tunneling from atomic tips (50), acoustic wave interactions (51), and so on.

Variable Capacitance. As a sensing mechanism, variable capacitance is very straightforward. As implied by Eq. (5), a change in the gap spacing or electrode area causes a change in capacitance. There is a multitude of mechanisms for sensing this change in capacitance, such as using a bridge circuit or using switched capacitance techniques (52,53).

Changes in capacitance also form a basic actuation mechanism. The electromechanical energy transduction associated with such systems can be examined by accounting for energy conservation in the electromechanical system. In the case of a simple capacitive system, the electrostatic co-energy can be found as the integral of (54):

$$dW'_{\mathrm{e}} = q \cdot dv + f^{\mathrm{e}} \cdot dx \tag{6}$$

where q and v are the charge and voltage on the capacitor, f^{e} is the force of electrical origin, and x is the direction of motion. In the electrically linear case where voltage is the independent variable, integration of Eq. (6) yields

$$f^{\mathrm{e}} = \frac{\partial W'_{\mathrm{e}}(v, x)}{\partial x} = \tfrac{1}{2} v^2 \frac{dC}{dx} \tag{7}$$

This relationship forms the basis for the electrostatic actuation in micromachined devices (55). Clearly this relation can be generalized to any number of electromechanical transduction elements or degrees of freedom (54). If we substitute the relation for the infinite parallel plate capacitor, Eq. (5), into Eq. (7), we find

$$f^{\mathrm{e}} = -\frac{v^2 \epsilon A}{2g^2} \tag{8}$$

What is important to note here is that the force is a function of the square of the capacitive gap spacing. In cases where the mechanical restoring force is a linear spring (as would be the case for devices with beam tethers, for example), the system will become unstable at some value of the gap spacing (56).

For small motions about an operating position, the electrostatic force can be linearized:

$$f^{\mathrm{e}} = -\frac{v^2 \epsilon A}{2(g + \Delta x)^2} \approx -\frac{v^2 \epsilon A}{2g^2}\left(1 - 2\frac{\Delta x}{g}\right) \tag{9}$$

where Δx is an incremental motion in one of the capacitor plates. This allows the electrostatic force to be cast in the form of an electrostatic spring constant:

$$k_{\mathrm{e}} = \frac{\Delta f^{\mathrm{e}}}{\Delta x} = \frac{v^2 \epsilon A}{g^3} \tag{10}$$

Note that this electrostatic spring acts in opposition to the mechanical spring.

Piezoresistance. Piezoresistance is the change in electrical resistivity of a material due to mechanical stresses. Semiconductors, such as silicon and germanium, show a particularly large piezoresistive effect which is more than an order of magnitude higher than that of metals. Hence, piezoresistance is frequently used as a sensing mechanism in micromachined devices. The geometry and placement of the piezoresistors are easily defined by selectively doping the semiconductor surface or by depositing a piezoresistive thin film on a nonsilicon surface. The ability to diffuse the dopant into the surface or deposit a thin film (i.e., polysilicon) allows the fabrication of thin piezoresistive layers (0.5 μm to 3.0 μm, for example). This allows the current to be restricted to the volume of maximum stress and thus yields the maximum signal.

The piezoresistive effect is an anisotropic relation between the stress tensor and the relationship between the electric field and the current density at a point. A full mathematical description of piezoresistance is beyond the scope of this article. The reader is referred to Sze (10) or Middelhoek (57) for a mathematical treatment. The relationship between electric field and current density can be written as

$$\frac{E_i}{\rho_0} = J_i + \pi_{ijkl}\sigma_{kl}J_j \tag{11}$$

where E is the electric field, ρ_0 is the unstrained resistivity, J is the current density, σ is the stress tensor, and π is the fundamental piezoresistive coefficient. Due to the cubic symmetry of silicon, π can be reduced to a 6-by-6 matrix with only three independent coefficients. The values of these coefficients for silicon are shown in Table 3 (58). Of all the orientations of stress and current that can be described by Eq. (11), two are particularly useful, the longitudinal and transverse components. To examine these, we can write the change in resistance in a piezoresistor as

$$\frac{\Delta R}{R} = \sigma_1 \pi_1 + \sigma_t \pi_t \tag{12}$$

where σ_{l} is stress component parallel to the direction of the current, σ_{t} is stress component perpendicular to the direction of the current, π_{l} is the longitudinal piezoresistance coefficient, and π_{t} is the transverse piezoresistance coefficient. Table 4 shows these piezoresistance coefficients as a function of various crystal orientations and the fundamental material parameters of Table 3.

Two canonical piezoresistive sensing structures are the diaphragm, typically used for pressure sensing, and the cantilever beam-proof mass, typically used for inertial sensing. Schematic cross-sectional drawings of these structures are shown in Figs. 8 and 9. In the diaphragm structure, piezoresistors are typically placed near the center of the diaphragm edge where the stress is highest [see Eq. (2)]. In the cantilever structure, the maximum stress caused by the deflection of the proof mass is at the beam surface.

A typical resistor configuration is the Wheatstone Bridge. In this configuration, two resistors are oriented so that they are most sensitive to stresses along their current carrying axis. Two more resistors are oriented to be most sensitive to stresses at right angles to their current flow. Thus, the resistance change of each pair is opposite. When electrically connected in a Wheatstone Bridge circuit, a large differential output voltage, which is independent of the absolute value of the piezoresistor's resistance, is obtained. One difficulty with piezoresistive sensors is their large temperature sensitivity.

Table 3. Piezoresistive Coefficients for *n*- and *p*-Type Silicon at Room Temperature (56)

Silicon	ρ_0 (Ω-cm)	π_{11} (10^{-11} Pa^{-1})	π_{12} (10^{-11} Pa^{-1})	π_{44} (10^{-11} Pa^{-1})
n-Type	11.7	−102.2	53.4	−13.6
p-Type	7.8	6.6	−1.1	138.1

These effects can be reduced by use of Wheatstone bridge circuits and careful resistor matching (10).

Piezoelectricity. Piezoelectricity relates to the crystalographic strains and polarization charge of an ionic crystal. When external force is applied to a piezoelectric crystal, a polarization charge is induced on the surface. If the force is time-varying, this polarization charge can be sensed as a time-varying voltage or current. Similarly, if an electric potential is applied, the crystal is deformed. The mathematical description of piezoelectricity is a description of the coupling terms that enter the stress–strain and polarization–electric-field relations. The reader is referred to Madou (10) for an introduction to these relations or to Auld (59) for a more in-depth treatment.

The most common piezoelectric materials used in micromachined devices are crystalline quartz, ceramics such as zinc oxide, lead zirconate titanate (PZT), barium titanate, and lead niobate, and polymers such as polyvinylidene fluoride (PVDF). Piezoelectric materials are most often used as actuators because they are capable of producing high stresses (but low strains) and can achieve large forces with a small amount of input power. Piezoelectric sensors often use a bimorph beam structure whose output is proportional to the bending of the bimorph.

Thermal Mechanisms. Thermal sensing can be divided into methods that directly produce an electrical signal and those that are mediated by another, typically mechanical, mechanism. Direct electrical transduction occurs with thermocouples, temperature-dependent resistors, and the various transistor-based mechanisms (60). Mechanically mediated mechanisms typically take advantage of the thermal expansion of a material or the difference in expansion of two bonded materials (bimorph) to achieve a mechanical stress or deformation. This mechanical signal is then measured with one of the mechanisms above such as a piezoresistor. Thermal actuation is also mechanically mediated as in the case where a bimorph is used to generate forces. Other actuation mechanisms take advantage of the large forces associated with a liquid–gas phase change.

Table 4. Longitudinal and Transverse Piezoresistance Coefficients for Various Directions in Cubic Crystals (after Ref. 9)

Longitudinal Direction	π_l	Transverse Direction	π_t
[1 0 0]	π_{11}	[0 1 0]	π_{12}
[0 0 1]	π_{11}	[1 1 0]	π_{12}
[1 1 1]	$\frac{1}{3}(\pi_{11} + 2\pi_{12} + 2\pi_{44})$	[1 −1 0]	$\frac{1}{3}(\pi_{11} + 2\pi_{12} - \pi_{44})$
[1 1 0]	$\frac{1}{2}(\pi_{11} + \pi_{12} + \pi_{44})$	[1 1 1]	$\frac{1}{3}(\pi_{11} + 2\pi_{12} - \pi_{44})$
[1 1 0]	$\frac{1}{2}(\pi_{11} + \pi_{12} + \pi_{44})$	[0 0 1]	π_{12}
[1 1 0]	$\frac{1}{2}(\pi_{11} + \pi_{12} + \pi_{44})$	[1 −1 0]	$\frac{1}{2}(\pi_{11} + \pi_{12} - \pi_{44})$

After Ref. 10, p. 166.

Resonant Sensing. Another general sensing mechanism is resonant sensing. Here an energy storage element is driven to resonance by a feedback mechanism. The system is designed so that variations in the quantity of interest alter the resonant frequency of this feedback system. This change in frequency is then measured and converted to an output signal. Since frequencies can be measured with high accuracy, very high precision sensors can often be realized using this technique (61). Actuators can also make use of the large stored energy in a resonant system to obtain large nonvibratory motions from small vibratory motions (62).

Viscous Damping. Although not a sensing mechanism, damping is a very important physical phenomenon in micromachined devices. Because of the small dimensions of micromachined devices, surface forces, such as viscous fluid damping, tend to dominate over momentum-based forces. From a fluid mechanics point of view, micromachined devices operate in low Reynolds number regimes, even for large velocities. There are approximations to the full Navier–Stokes equations which often apply to micromachined devices. For example, for plate-like structures that move laterally over each other, the approximations of Stokes and Couette flow shear damping are appropriate (63). For parallel plates that move toward (or away from) each other, a squeeze-flim damping model is appropriate (64). Since micromachined devices operate in a low Reynolds number regime, the damping can be quite large when the device operates in liquids or in atmospheric pressure gas. For low-bandwidth devices, this damping can be helpful. However, high-bandwidth and resonant devices typically require evacuated packaging to achieve the required high values of the quality factor.

MICROMACHINED DEVICES

The breadth of micromachined devices that have been proposed or demonstrated is large and continues to grow. A general characteristic of these devices is that they interact or facilitate interaction across physical domains. Cataloging these devices can be quite difficult since they span a broad range of physical domains. However, these devices can, in general, be characterized as either sensors or actuators. Sensors typically translate energy from the energy domain being sensed into a signal (typically electrical), possibly through intermediate domains. Actuators, on the other hand, typically convert an electrical signal into an energy or action in the physical domain to be actuated. As can be seen from the similarity of these definitions, both sensors and actuators are fundamentally the same thing: transducers of energy from one physical domain to another. The real distinction between a sensor and an actuator is one of intent. And of course, there are devices which contain elements of both, such as the force re-balance accelerometer which uses actuation driven by a feedback loop to null balance the sensor.

The commercial successes of micromachined devices remain few, mostly due to manufacturing reproducibility problems and packing complexity. The successes mostly fall into the category of sensors. The following sections overview many of the broad classes of micromachined sensors and actuators.

Pressure Sensors

The silicon micromachined pressure sensor was one of the first commercially successful micromachined devices. As late as 1989, bulk micromachined pressure sensors accounted for most of the revenue in silicon micromachined sensors. Most of the silicon pressure sensors manufactured today are for automobile applications, most notably the manifold absolute pressure (MAP) sensor. These pressure sensors can sense relative to a vacuum or relative to a fixed pressure such as atmospheric, or they can be differential.

The general functional characteristic of the pressure sensor is quite simple. Applied pressure causes a thin-film diaphragm to deflect. The deflection is then sensed, typically by one of two methods: capacitive or piezoresistive. Figure 8 shows a schematic cross section of a bulk micromachined, silicon diaphragm pressure sensor. Piezoresistively sensed devices place a piezoresistor at one or more locations which encounter maximum stress when the diaphragm deflects. The piezoresistors are often placed in a bridge circuit to increase sensitivity. In the case of a capacitive sensor, the deflection of the diaphragm changes the gap between it and a counterelectrode (not shown). The change in capacitance is sensed electronically.

Piezoresistive sensing is simple and requires little, if any, external circuitry. Capacitive sensing requires an external circuit; and in the case where this circuit is not integrated on the same piece of silicon as the diaphragm, the capacitance must be large enough to be sensed in the presence of the large parasitic capacitance associated with the interconnection to the circuit. These issues often cause capacitive sensors to be more expensive to produce. However, capacitive sensing is inherently more sensitive and significantly less temperature-dependent than piezoresistive sensing. Thus, for many applications, where the sensor will see significant temperature variations in its environment, capacitive sensing is chosen.

Inertial Sensing

Inertial sensing implies the sensing of inertial forces such as acceleration, gravitation, or angular acceleration. Current commercial examples are accelerometers and gyroscopes, or angular rate sensors, used in automobile and military applications. Other related applications are shock sensors, vibration sensors, and gravitometers.

Accelerometers. Accelerometers have seen their largest market in automobile airbag sensing. Micromachined accelerometers have found a niche here because of their ability to be cheaply produced in large volumes. This has given them a significant advantage over their larger electromechanical predecessors.

The majority of micromachined accelerometers work in a similar manner. They are constructed as a proof mass and spring system. When the device is subject to an acceleration load, the proof mass moves. This motion is typically sensed by capacitive or piezoresistive means. A good figure of merit for accelerometers is the resonant frequency of the sensitive mode [see Eq. (3)]. In most cases, the accelerometer output is proportional to the displacement of the proof mass. Thus, the scale factor is proportional to one over the square of the resonant frequency. Hence, a lower resonant frequency yields a more sensitive device for a given proof mass deflection to output gain.

Bulk micromachined accelerometers have the advantage of a large proof mass which can be as thick as the wafer from which it is constructed. In fact, wafer-bonded structures allow the proof mass to be multiple wafer thicknesses. As with bulk pressure sensors, the deflection of the proof mass can be measured capacitively with an adjacent counterelectrode. In the case of piezoresistive sensing, piezoresistors are typically placed on the tether springs which support the proof mass (see Fig. 9). Since the proof mass is thick and thus rigid, the tethers are the only part of the structure where significant strains are obtained. The tethers in this type of system are typically thin beams which are left unetched during the silicon etch, or are made from a thin film which was patterned and etched prior to the proof mass etch.

Surface micromachined accelerometers are thin-film planar devices. They can move perpendicular to the plane of the proof mass, as bulk micromachined accelerometers do, or they can move in the plane. In the perpendicular case, they can use capacitive sensing in an analogous fashion as the bulk structures. The mass of a surface micromachined structure is typically much smaller than a bulk micromachined structure. Thus, to keep the resonant frequency of a surface micromachined accelerometer at an acceptably low value, the tethers must be significantly more compliant. As a consequence, the strain level in the thethers will be small and usually insufficient for piezoresistive sensing.

In the case of lateral, or in-plane, accelerometers, the capacitive counter electrodes must be in the same plane as the proof mass motion. This implies that the "plates" are formed by the edge of the structural layer's thin-film material. In order to obtain sufficient capacitance for sensing, interdigitated fingers are used to increase the capacitor electrode area and thus the variable capacitance. Figure 6 shows a SEM of the Analog Devices ADXL76 accelerometer. This is an example of a surface micromachined accelerometer showing the interdigitated finger electrodes.

Given the basic accelerometer structure and sensing mechanism, there are many ways to construct the sensing system. A fundamental difference is the closed-loop versus the open-loop system. In an open-loop system, the proof mass is free to deflect according to the applied acceleration and the tether's compliance. In a closed-loop system, a feedback loop applies a force to the proof mass which balances the inertial force and keeps the proof mass close to its zero acceleration position. The output of the sensor is then proportional to the magnitude of the feedback signal. The benefits of such a scheme are that the sensor will avoid any nonlinearities associated with large proof mass deflections. However, this comes at the expense of a more complicated, larger, and more expensive to produce circuit.

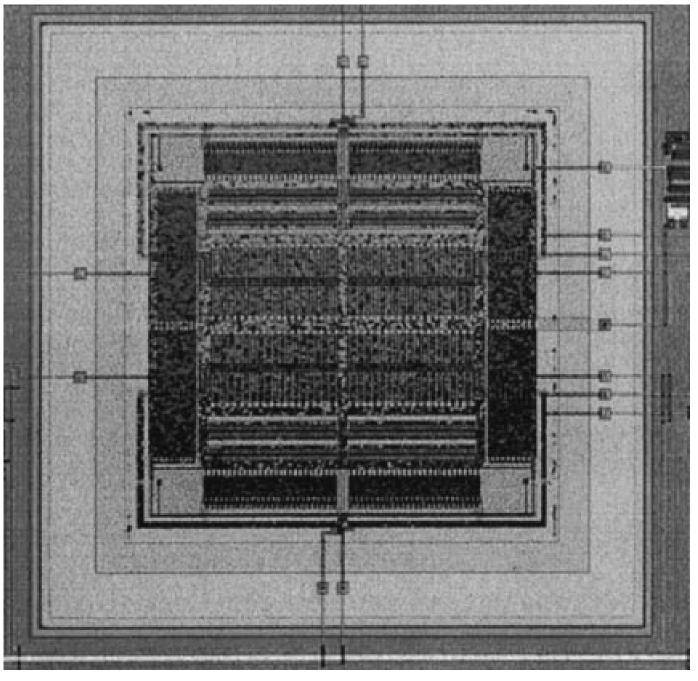

Figure 14. A photomicrograph of a surface micromachined vibratory gyro. The device is driven into resonance in the up/down axis. An angular rate about the out-of-plane axis produce a coriolis acceleration in the left/right axis which is sensed as a left/right motion. (From Ref. 66.)

Other types of accelerometers have been devised. In particular, the resonant accelerometer is of interest because of its potential for high accuracy. In a typical resonant accelerometer, the motion of a proof mass caused by the acceleration causes the stiffness of a resonant beam to change. This, in turn, causes its resonant frequency to change. Another type of accelerometer is the tunneling accelerometer (65). Here displacements of a proof mass are measured with high precision by measuring the tunneling current between a sharp tip and an adjacent ground plane. Micromachining techniques are well suited to fabricating tips with appropriately small tip radii.

Gyroscopes. Another important class of inertial sensor is the gyroscope or angular rate sensor. The most familiar type of gyroscope is the rotating disk gyro. However, this type of free rotational motion remains impractical for micromachined devices. More practical for micromachined devices is the vibrating gyro. The fundamental operating principle is the sensing of Coriolis acceleration:

$$a_c = 2\Omega \times v \tag{13}$$

where a_c is the Coriolis acceleration, Ω is the angular rate, and v is velocity of the proof mass. This velocity is usually obtained as the vibration of a spring-mass system in an oscillatory feedback loop. The Coriolis acceleration then acts on the inertial mass to generate a motion which is sensed.

Figure 14 shows a vibratory rate gyroscope which is sensitive to rotation rates about the direction perpendicular to the plane of the structure (z axis) (66). The moving mass is driven into resonance in the left–right, in-plane direction (x axis). Rotations in the z axis cause y-axis-directed forces. The y-axis-directed motions are sensed capacitively in the same manner as the lateral accelerometer described above.

Although the vibratory gyro avoids many of the problems associated with rotating gyros, its concept is based on the assumption of an ideal lossless vibrating member with perfect symmetry. In a practical case, the most obvious loss mechanism is viscous damping. This can be eliminated or reduced by operation in a vacuum. This requires a stable vacuum package which is difficult and expensive to produce (67). Also of significance are acoustic losses into the body to which the gyro is fixed (i.e., the substrate). Such coupling can lead to linear accelerations or vibrations appearing as rate signals. Constructing a balanced oscillator in which reactions to the driving force are not felt by the device's mountings can reduce these losses (68).

In addition to vibrating mass structures as described above, there is a class of structures which use rings or thin axisymmetric shells as the vibrating structures. Figure 15 shows a vibrating ring gyro made with electroplated nickel (69). Vibrating shell gyros pick off the rotation of a vibrational mode's antinode position, which is caused by the input rotation rate. Note that the rotation of the antinodes corresponds to a rotation-induced transfer of energy between two identical vibrational modes (70). In vibrating mass gyros, the output signal depends on the rotation-induced transfer of energy between two different vibration modes. This difference allows the vibrating shell gyro to avoid the temperature sensitivities caused by different temperature variations in the vibration modes of the vibrating mass gyro.

Thermal Sensors

There are a large number of thermal sensors which are silicon-based, including the temperature-sensing capabilities of the transistor itself. Here we will focus on those thermal devices that rely on micromachining for their function.

Thermal flow sensors are often based on the idea that a fluid, which flows past a hot surface, will carry heat away from the surface. A typical micromachined device using this type of mechanism is the flow anemometer. Here, a temperature-dependent resistor is used to detect the heat lost to the flow from a resistive heat source. The rate of heat loss is proportional to the flow velocity. A related mechanism uses two thermally isolated elements. The first is a heater, which provides a pulsed heat flux. The second is a downstream temperature sensor which detects the heat pulse generated by the upstream heater. The fluid velocity is given by the time of flight (10). Figure 16 shows a characteristic implementation (71). The heater and the sensor are suspended in the center of the flow channel by thin, thermally isolating supports. The thermal sensing element is often a temperature-dependent resistor in a bridge configuration. The IR bolometer is another device that uses an isolated thermal resistor (72).

Another basic construction is the stress-based thermal sensor. Here two material layers with different thermal expansion coefficients are used to form a bimorph structure that exhibits a bending moment that is a function of the temperature of the device. Examples include IR sensors where the heating caused by the IR energy flux causes a deflection. Thermal actuation devices are also based on the bimorph effect. Thermally actuated valves have been built that take ad-

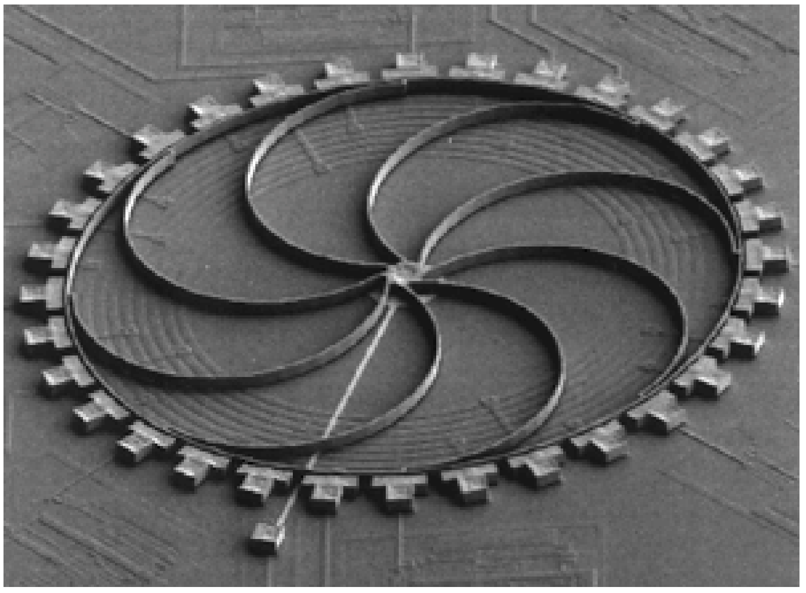

Figure 15. A scanning electron micrograph of a ring gyro device. The ring is driven into resonance by the surrounding electrodes (T-shaped structures). An angular rate about the out-of-plane axis causes a shift in the position of the vibration nodes which is sensed (capacitively) by the surrounding electrodes. (From Ref. 69.)

vantage of the large forces associated with a liquid–gas phase change (73). Other examples include the actuation of optical mirror devices (74) and thermally driven resonators.

Chemical and Biological Sensors

A full discussion of chemical and biological sensors is an intricate one that is far beyond the scope of this article. However, it is worth pointing out a few common threads. These sensors can be categorized into devices which detect gases, devices which detect liquids, and devices which detect complicated biological molecules such as DNA or proteins. One thing to note is that most of these sensors do not rely fundamentally on micromachining for their construction. The fundamental functional mechanisms are typically surface chemical in nature (often requiring catalysts, etc.). To date, most innovation in these systems has come from exploration of chemical reactions and materials. Semiconductor and micromachined device fabrication techniques simply provide a way of making the devices smaller, cheaper, faster, etc. These chemical issues are beyond the scope of this article. The reader is referred to Ref. (10) for a discussion of these issues.

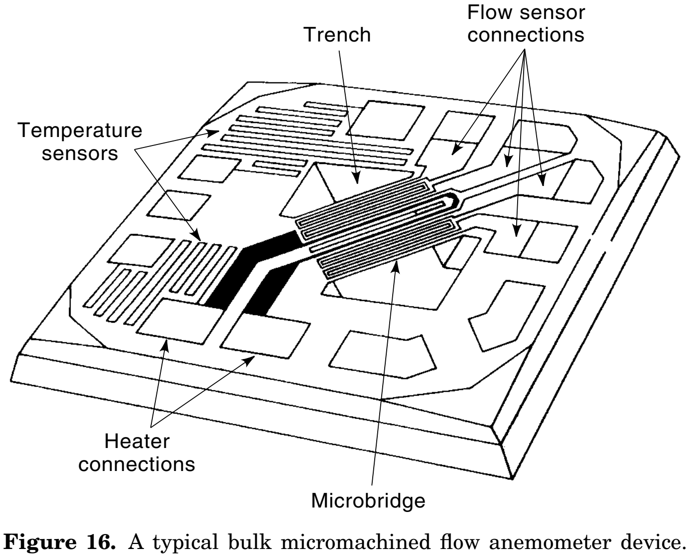

Figure 16. A typical bulk micromachined flow anemometer device. Heat is generated by a resistive element (black) and sensed by the upstream and downstream flow sensor elements. (After Ref. 71.)

The detection of combustible gases such as CO, H_2, alcohols, hydrocarbons, and so on, is most frequently performed with either semiconducting metal oxides or field-effect transistors (FETs). In the case of the metal oxide semiconductors, a surface reaction occurs between oxygen and the gas, which changes the resistance of the semiconductor. In the case of the FET, a reaction occurs on the surface over the channel, which alters the potential at the "gate" and modulates current flow in the channel. This same FET mechanism can be used to detect ionic species. Biosensors are an extension of chemical sensors, which rely on biological materials and biochemical reactions. These reactions have the benefit of high selectivity and sensitivity. Thus a biosensor can be described as the addition of a biological sensing mechanism to a chemical (or physical) transducer.

One fundamental difficulty with both chemical and biological sensors is that they must come into contact with the chemical or biological environment they wish to sense. It is difficult to make them reversibly reactive to the desired species while, at the same time, unreactive to other species present in the environment. Selectively permeable membranes and arrays of sensors have been used to overcome this problem.

Micromachined Actuators

Actuators have long been envisioned as allowing the true revolution in micromachined devices. To date, however, their use has been limited. The most widespread use of actuation is in force feedback inertial sensors (6). One of the first devices that constituted an actuator in its own right was the so-called micromotor. These devices were typically rotary, variable-capacitance motors as shown in Fig. 17 (75). Variable capacitance was chosen as a drive mechanism because of its compatibility with micromachining processes and materials.

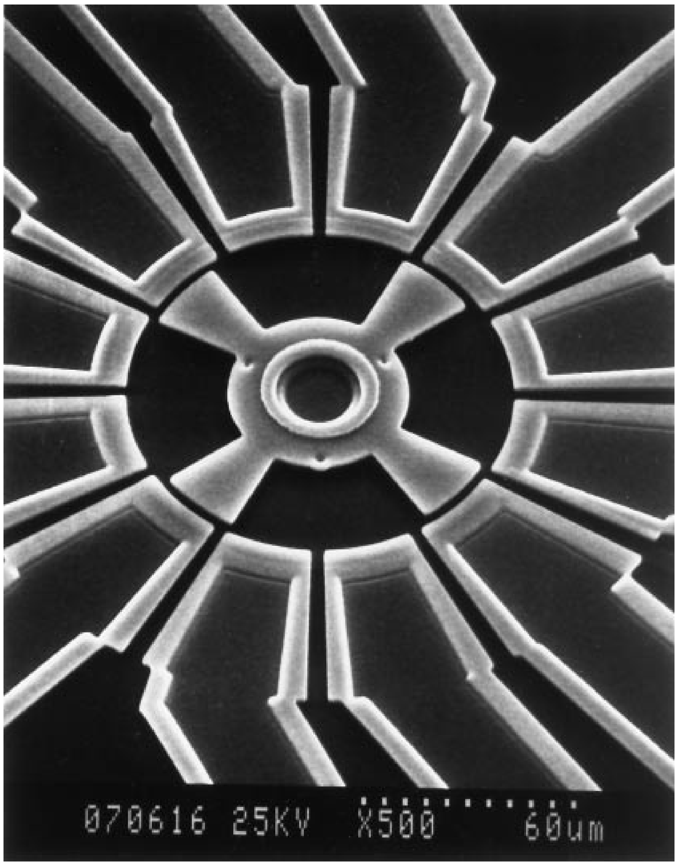

Figure 17. A scanning electron micrograph of a salient-pole variable-capacitance micromotor. Attractive electrostatic forces between the rotor poles and the fixed stator poles (around the periphery) cause rotary motion. (Courtesy of MCNC.)

However, electrostatic systems have some scaling advantages over magnetic systems as the characteristic length decreases to the micron range (55). The most significant difficulty in the construction of such devices is the formation of a bearing structure that can restrain the rotor to rotational motion without significant friction or wear. Because of this difficulty, and in an effort to overcome such friction (as well as viscous air damping), various motor configurations have been constructed (76). In spite of these design variations, micromachined motors continue to suffer from short lifetimes due to wear. Also, they suffer from restricted usefulness due to the relatively high applied voltages required to overcome friction and supply useful output torque.

Electrostatic linear actuators have also been developed. Devices with relatively unconstrained linear motion suffer from many of the same problems as their rotary predecessors. Constrained motion devices—that is, actuators whose moving member is supported and whose limited motion is typically due to a balance between the electrostatic drive force and an elastic restraint—have been more successful. Such devices form the basis for resonant sensors, where the spring support and the moving mass form the resonant system (77). Hybrid systems have also been developed such as impact systems which use a resonator to strike a second moving mass (for example, a rotor) and cause it to move (78). Repeated, high-frequency impacts yield quasi-continuous motion. Another related concept is the use of electrostatic forces to modulate the effective stiffness and hence resonant frequency of a spring-mass resonant system (79).

One class of constrained motion actuating devices is the optical mirror and optical grating devices. The simplest type is the torsional mirror device (80). Here a mirror, supported on a torsional tether, is actuated to control the angle of reflection of a laser beam or other light source. Both continuous and bi-stable control have been used. Various devices which use thin cantilever beams or bridges to form controllable defraction gratings have been demonstrated (81).

The use of piezoelectric materials in actuator devices is very common due to their ability to provide large forces and small displacements with low applied voltages. Typical applications are fluid pumps (82), linear and rotary motors (83), and surface acoustic wave (SAW) sensors (10).

Another device, which has garnered considerable interest, is the micromachined switch, or relay. The ability to achieve a true open circuit switch, integrated with electronics could be very useful for integrated circuit testing devices, communications systems, and RF systems. Simple electrostatically actuated cantilever beams or bridges have been designed for this purpose (84). The difficulty with these structures, as with macroscopic switches, are the material properties of the contacting surfaces. Their sticking properties and their ability to withstand millions of open/close cycles is critical.

Software Design Tools for Micromachined Devices

The design of micromachined devices involves examining devices that operate in a broad set of physical domains. The 3-D nature of micromachined devices typically requires full 3-D numerical simulation based on the Finite Element Method (FEM) or the Boundary Element Method (BEM). FEM and BEM tools for specific physical domains, such as mechanics or magnetics, were developed for macroscopic systems. Although these tools can provide useful simulation results for some types of uncoupled behavior, micromachined devices usually perform a transduction of energy between one physical domain and another which often requires the solution of coupled physics problems (85). In this case, coupled physical domain solvers are required. A classic example for micromachined devices is the electrostatic instability of a bending beam electrode above a ground plane. As a voltage is applied to the electrode, a force develops between the electrode and the ground plane. This causes the beam to bend, closing the gap between the electrode and the ground plane. This, in turn, causes the force to increase, which bends the beam some more. At some “pull-in” voltage, this interaction is unstable and the beam collapses down to the ground plane. Knowledge of this pull-in voltage is often an important design parameter. Simulation of this value requires that the mechanics and the electrostatics of this system be solved together in a coupled, self-consistent way. There are many other coupled domains that are relevant to micromachined devices, such as magnetomechanics and fluid–structure interaction. Work on micromachined devices has accelerated efforts to develop coupled solvers for these domains.

From the perspective of a design tool environment, MEMS involve making 3-D mechanical devices with the manufacturing techniques of integrated circuit fabrication. This creates a need for design tools that join the functionality of 3-D mechanical design tools (MDA) with integrated circuit design tools (EDA). For example, 3-D micromachined devices are typically generated photolithographically from a series of 2-D layout masks. The masks are made in an EDA layout editor. However, FEM-based simulations require a 3-D solid model as would be generated in a MDA solid model editor. Micromachined device design software environments such as MEMCAD (46) bridge this gap by generating the 3-D solid model directly from the 2-D layout masks and a description of the fabrication process. In addition, micromachined devices are most often used within a larger system which typically contains one or more micromechanical elements and circuit elements. In order to simulate such complex systems in a reasonable amount of time, the FEM/BEM-based device model must, in general, be reduced to a lower-order lumped model (86). Software tools which automatically produce such low-order models are beginning to appear (46).

Another important area for simulation is the interaction of the MEMS system with the package. Integrated circuits interact with their packages primarily through thermal dissipation and the mechanical stresses caused by thermal expansion coefficient mismatches. Due to their mechanical nature, micromachined devices are typically even more susceptible to these issues. In addition, many micromachined devices, such as pressure or flow sensors, must interact directly with their environment. Thus, the MEMS designer often has to design application-specific packaging. Optimizing such coupled MEMS/package systems requires considerable simulation. These application-specific packages are often more expensive than the underlying MEMs device. Therefore, an optimized package/device design can be critical to overall price and performance.

Further Reading

The reader is directed to several books and chapters discussing micromachining technology (10). Other very useful books are listed in the Reading List. The two major journals of the field are the IEEE *Journal of Micro Electromechanical Systems* (JMEMS) and *Sensors & Actuators.* Although there are at least 10 conferences that discuss micromachined devices, the three major conferences are the *International Conference on Solid-State Sensors and Actuators* (Transducers), *The Solid-State Sensor and Actuator Workshop,* and the *International Workshop on Micro Electro Mechanical Systems* (MEMS).

BIBLIOGRAPHY

1. S. Wolf and R. N. Tauber, *Silicon processing for the VLSI era,* Vol. 1, *Process technology,* Sunset Beach, CA: Lattice Press, 1986.
2. O. N. Tufte, P. W. Chapman, and D. Long, Silicon diffused element piezoresistive diaphragms, *J. Appl. Phys.,* **33**: 3322, 1962.
3. Editorial, *Thermal Character Print Head,* Austin: Texas Instruments, 1977.
4. E. Bassous, H. H. Taub, and L. Kuhn, Ink jet printing nozzle arrays etched in silicon, *Appl. Phys. Lett.,* **31**: 135–137, 1977.
5. P. O'Neill, A monolithic thermal converter, *Hewlett-Packard J.,* **31**: 12–13, 1980.
6. S. J. Sherman et al., A low cost monolithic accelerometer: Product/technology update, *IEEE Int. Electron Devices Meet.,* San Francisco, 1992, pp. 501–504.
7. B. Studer and W. Zingg, Technology and characteristics of chemically milled miniature quartz crystals, *4th Eur. Freq. Time Forum,* Neuchatel, Switzerland, 1990, pp. 653–658.
8. K. E. Peterson, Silicon as a mechanical material, *Proc. IEEE,* **70**: 420, 1982.
9. J. S. Danel, F. Michel, and G. Delapierre, Micromachining of quartz and its applications to an acceleration sensor, *Sensors Actuators,* **A21-A23**: 971, 1990.
10. S. M. Sze (ed.), *Semiconductor Sensors,* New York: Wiley, 1994; M. Madou, *Fundamentals of Microfabrication,* Boca Raton, FL: CRC Press, 1997.
11. H. L. Seidel et al., Anisotropic etching of crystalline silicon in alkaline solutions: I. Orientation dependence and behavior of passivation layers, *J. Electrochem. Soc.,* **137**: 3612, 1990.
12. H. L. Seidel et al., Anisotropioc etching of crystalline silicon in alkaline solutions: II. Influence of dopants, *J. Electrochem. Soc.,* **137**: 3626, 1990.
13. A. Reisman et al., The controlled etching of silicon in catalyzed ethylene-diamine-pyrocathechol-water solutions, *J. Electrochem. Soc.,* **126**: 1406–1414, 1979.
14. O. Tabata et al., Anisotropic etching of silicon in TMAH solutions, *Sensors Actuators,* **A34**: 51–57, 1990.
15. C. Keller and M. Ferrari, Milli-scale polysilicon structures, *Tech. Dig., 1994 Solid State Sensor Actuator Workshop,* Hilton Head Island, SC, 1994, pp. 132–137.
16. G. Wallis and D. L. Pomerantz, Field assisted glass-metal sealing, *J. Appl. Phys.,* **40**: 3946, 1969.
17. T. R. Anthony, Anodic bonding of imperfect surfaces, *J. Appl. Phys.,* **54**: 2419–2428, 1983.
18. M. Shimbo et al., Silicon-to-silicon direct bonding method, *J. Appl. Phys.,* **60**: 2987, 1986.
19. W. H. Ko, J. T. Suminto, and G. J. Yeh, Bonding techniques for microsensors, in C. D. Fung et al. (eds.), *Micromachining and Micropackaging of Transducers,* Amsterdam: Elsevier, 1985, pp. 41–61.
20. E. J. J. Kruglick, B. A. Warneke, and K. S. J. Pister, CMOS 3-axis accelerometers with integrated amplifier, *Proc. IEEE Micro Electro Mechn. Syst. Workshop (MEMS '98),* Heidelberg, 1998, pp. 631–636.
21. D. L. Klein and D. J. D'Stefan, Controlled etching of silicon in the HF–HNO_3 system, *J. Electrochem. Soc.,* **109**: 37–42, 1962.
22. L. S. Fan, Y.-C. Tai, and R. S. Muller, Integrated movable micromechanical structures for sensors and actuators, *IEEE Trans. Electron Devices,* **35**: 724–730, 1988.
23. H. C. Nathanson et al., The resonant gate transistor, *IEEE Trans. Electron Devices,* **ED-14**: 117–133, 1967.
24. R. T. Howe and R. S. Muller, Resonant polysilicon microbridge integrated with NMOS detection circuitry, *IEEE Int. Electron Devices Meet.,* San Francisco, 1984, pp. 213–216.
25. T. A. Core, W. K. Tsang, and S. J. Sherman, Fabrication technology for an integrated surface-micromachined sensor, *Solid State Technol.,* **October**: 39–44, 1993.
26. L. J. Hornbeck, Deformable-mirror spatial light modulators, *SPIE Crit. Rev.,* **1150**: 86, 1989.
27. G. T. Mulhern, S. Soane, and R. T. Howe, Supercritical carbon dioxide drying for microstructures, in *1993 Int. Conf. Solid-State Sensors Acuators (Transducers '93),* Yokohama, Japan: p. 296.
28. H. Guckel, J. J. Sniegowski, and T. R. Christenson, Advances in processing techniques for silicon micromechanical devices with smooth surfaces, in *1989 Int. Workshop on Micro Electromechanical Systems (MEMS '89),* Salt Lake City, UT: p. 71.
29. U. Srinivasan, M. R. Houston, R. T. Howe, and R. Maboudian, Self-assembled fluorocarbon films for enhanced silicon reduction,

1997 Int. Conf. Solid-State Sensors Actuators (Transducers '97), Chicago, IL: pp. 1399–1402.

30. H. Guckel, T. Randazzo, and D. W. Burns, A simple technique for the determination of mechanical strain in thin films with application to polysilicon, *J. Appl. Phys.,* **57**: 1671–1675, 1985.
31. R. T. Howe and R. S. Muller, Polycrystalling silicon and amorphous silicon micromechanical beams: Annealing and mechanical properties, *Sensors Actuators,* **4**: 447–454, 1983.
32. M. Biebl, G. T. Hulhern, and R. T. Howe, Low in-situ phosphorous doped polysilicon for integrated MEMS, *8th Int. Conf. Solid-State Sensors Actuators (Transducers 95),* Stockholm, Vol. 1, 1995, pp. 198–201.
33. H. Guckel et al., The application of fine-grained tensile polysilicon to mechanically resonant transducers, *Sensors Actuators* **A21-A23**: 346–350, 1990.
34. P. Krulevitch and G. C. Johnson, Stress gradients in thin films used in micro-electro-mechanical systems, *ASME Winter Annu. Meet.,* New Orleans, LA, 1993, DSC-46: pp. 89–95.
35. J. H. Smith et al., Embedded micromechanical devices for the monolithic integration of MEMS with CMOS, *Int. Electron Devices Meet.,* Washington, DC, 1995, pp. 609–612.
36. J. M. Bustillo et al., Process technology for the modular integration of CMOS and polysilicon microstructures, *Microsyst. Technol.,* **1**: 30–41, 1994.
37. K. S. J. Pister et al., Microfabricated hinges: 1 mm vertical features with surface micromachining, *Tech. Dig., 6th Inter. Conf. Solid-State Sensors Actuators (Transducers '91),* 1991.
38. T. Masaki, K. Kawata, and T. Masuzawa, Micro electro-discharge machining and its applications, *Proc. IEEE Micro Electro Mech. Syst. Workshop (MEMS '90),* Napa, CA, 1990, pp. 21–26.
39. M. J. Vasile, C. Biddick, and A. S. Schwalm, Microfabrication by ion milling: The lathe technique, *J. Vac. Sci. Technol.,* **B12**: 2388–2393, 1994.
40. M. A. Moreland, Ultrasonic machining, in S. J. Schneider (ed.), *Engineered Materials Handbook,* Metals Park, OH: ASM International, 1992, pp. 359–362.
41. E. W. Becker et al., Production of separation nozzle systems for uranium enrichment by a combination of x-ray lithography and galvanoplastics, *Naturwissenschaften,* **69**: 520–523, 1982.
42. H. Guckel et al., Fabrication of assembled micromechanical components via deep x-ray lithography, *Proc., IEEE Micro Electro Mech. Syst. Workshop (MEMS '91),* Nara, Japan, 1991, pp. 70–74.
43. C. Burbaum et al., Fabrication of capacitive acceleration sensors by the LIGA technique, *Sensors Actuators,* **A25**: 559–563, 1991.
44. H. Guckel et al., A first functional current excited planar rotational magnetic micromoter, *Proc., IEEE Micro Electro Mech. Syst. Workshop (MEMS '93),* Fort Lauderdale, FL, 1993, pp. 7–11.
45. T. R. Christenson, J. Klein, and H. Guckel, An electromagnetic micro dynamometer, *Proc., IEEE Micro Electro Mech. Syst. Workshop (MEMS '94),* Amsterdam, 1994, pp. 386–391.
46. *Memcad 5.0 Users Manual,* Cambridge, MA: Microcosm Technologies, Inc., 1999.
47. S. P. Timoshenko and S. Woinowsky-Krieger, *Theory of Plates and Shells,* New York: McGraw-Hill, 1970, 2nd ed.
48. W. C. Young, *Roark's Formulas for Stress & Strain,* New York: McGraw-Hill, 1989, 6th ed.
49. M.-H. Kiang et al., Micromachined polysilicon microscanner for barcode readers, *IEEE Photon. Technol. Lett.,* **8** (12): 1707–1709, 1996.
50. J. Wang et al., Study of tunneling noise using surface micromachined tunneling tip devices, *Proc. 1997 Int. Conf. Solid-State Sensors Actuators (Transducers '97),* Chicago, 1997, Vol. 1, pp. 467–470.
51. B. A. Martin, S. W. Wenzel, and R. M. White, Viscosity and density sensing with ultrasonic plate waves, *Sensors Actuators,* **A21-A23**: 704–708, 1989.
52. J. T. Kung, H.-S. Lee, and R. T. Howe, A digital readout technique for capacitive sensor applications, *IEEE J. Solid-State Circuits,* **SC-23**: 972–977, 1988.
53. M. Lemkin, B. E. Boser, and D. Auslander, Fully differential lateral ΣΔ accelerometer with digital output, *Tech. Dig., 1996 Solid State Sensor Actuator Workshop,* Hilton Head Island, SC, 1996.
54. H. H. Woodson and J. R. Melcher, *Electromechanical Dynamics,* New York: Wiley, 1968, Part 1, Chap. 3.
55. S. F. Bart et al., Design considerations for microfabricated electric actuators, *Sensors Actuators,* **14**: 269–292, 1988.
56. P. M. Osterberg and S. D. Senturia, M-TEST: A test chip for MEMS material property measurement using electrostatically actuated test structures, *J. Microelectromech. Syst.,* **6**: 107–118, 1997.
57. S. Middelhoek and S. A. Audet, *Silicon Sensors,* London: Academic Press, 1989, Chap. 3.
58. C. S. Smith, Piezoresistance effect in germanium and silicon, *Phys. Rev.,* **94**: 42–49, 1954.
59. B. A. Auld, *Acoustic Fields and Waves in Solids,* Malabar, FL: Krieger Publishing, 1990, 2nd ed., Chap. 8.
60. L. Ristic (ed.), *Sensor Technology and Devices,* Boston: Artech House, 1994, Chap. 8.
61. R. T. Howe and R. S. Muller, Resonant microbridge vapor sensor, *IEEE Trans. Electron Devices,* **ED-33**, 499–506, 1986.
62. M. J. Daneman et al., Linear microvibromotor for positioning optical components, *Proc. IEEE Micro Electro Mech. Syst. Workshop (MEMS '95),* Amsterdam, 1995, pp. 55–60.
63. Y.-H. Cho, A. P. Pisano, and R. T. Howe, Viscous damping model for laterally oscillating microstructures, *J. Microelectromech. Syst.,* **3**: 81–87, 1994.
64. Y.-J. Yang and S. D. Senturia, Numerical simulation of compressible squeezed-film damping, *Tech. Dig., 1996 Solid State Sensor Actuator Workshop,* Hilton Head Island, SC, 1996, pp. 76–79.
65. H. K. Rockstad et al., A miniature high-sensitivity broad-band accelerometer based on electron tunneling transducers, *Sensors Actuators,* **A43**: 107–114, 1994.
66. W. A. Clark, R. T. Howe, and R. Horowitz, Surface micromachined Z-axis vibratory rate gyroscope, *Tech. Dig., 1996 Solid State Sensor Actuator Workshop,* Hilton Head Island, SC, 1996, pp. 283–287.
67. M. B. Cohn et al., Wafer-to-wafer transfer of microstructures for vacuum packaging, *Tech. Dig., 1996 Solid-State Sensor Actuator Workshop,* Hilton Head Island, SC, 1996, pp. 32–35.
68. C. H. J. Fox and D. J. W. Hardie, Vibratory gyroscopic sensors, in H. Sorg (ed.), *Proceedings of the Symposium on Gyro Technology,* Berln: Stuttgart, Germany: 1984, pp. 13.0–13.30.
69. M. W. Putty and K. Najafi, A micromachined vibrating ring gyroscope, *Tech. Dig., 1996 Solid-State Sensor Actuator Workshop,* Hilton Head Island, SC, 1994, pp. 213–220.
70. A. Lawrence, *Modern Inertial Technology,* New York: Springer-Verlag, 1993.
71. R. G. Johnson and R. E. Higashi, A highly sensitive silicon chip microtransducer for air flow and differential pressure sensing applications, *Sensors Actuators,* **11**: 63–72, 1987.
72. W. Lang, K. Kuhl, and E. Obermeier, A thin-film bolometer for radiation thermometry at ambient temperature, *Sensors Actuators,* **A21-A23**: 473–477, 1990.
73. M. J. Zdeblick et al., Thermopneumatically actuated microvalves and integrated electro-fluidic circuits, *Tech. Dig., 1994 Solid State Sensor Actuator Workshop,* Hilton Head Island, SC, 1994, pp. 251–255.

74. W. D. Cowan and V. M. Bright, Thermally actuated piston micromirror arrays, *Proc. SPIE,* **3131**: 1997.

75. S. F. Bart et al., Electric micromotor dynamics, *IEEE Trans. Electron Devices,* **39**: 566–575, 1992.

76. M. Mehregany et al., Principles in design and microfabrication of variable-capacitance side-drive motors, *J. Vac. Sci. Technol.,* **A8**: 3614–3624, 1990.

77. C. T.-C. Nguyen, Microelectromechancal devices for wireless communications, *Proc. IEEE Micro Electro Mech. Syst. Workshop (MEMS '98),* Heidelberg, 1998, pp. 1–7.

78. A. P. Lee, P. B. Ljung, and A. P. Pisano, Polysilicon micro vibromotors, *Proc. IEEE Micro Electro Mech. Syst. Workshop (MEMS '91),* Nara, Japan, 1991, pp. 177–182.

79. S. G. Adams, F. Bertsch, and N. C. MacDonald, Independent tuning of the linear and nonlinear stiffness coefficients of a micromechanical device, *Proc. IEEE Micro Electro Mech. Syst. Workshop (MEMS '96),* San Diego, CA, 1996, pp. 32–37.

80. J. M. Younse, Projection display systems based on the Digital Micromirror Device (DMD), *Proc. SPIE, Microelectron. Struct.,* **2641**: 64–75, 1995.

81. D. M. Bloom, Grating light valves for high resolution displays, *Tech. Dig., 1994 Int. Electron Devices Meet.,* San Francisco, 1994, p. 343.

82. H. T. G. Van Lintel, F. C. M. van der Pol, and S. Bouwstra, A piezoelectric micropump based on micromachining of silicon, *Sensors Actuators,* **15**: 153–167, 1988.

83. K. R. Udayakumar et al., Ferroelectric thin film ultrasonic micromotors, *Proc. IEEE Micro Electro Mech. Syst. Workshop (MEMS '91),* Nara, Japan, 1991, pp. 109–113.

84. S. Majumder et al., Measurement and modeling of surface micromachined, electrostatically actuated microswitches, *Proc. 1997 Int. Conf. Solid-State Sensors Actuators (Transducers '97),* Chicago, 1997, pp. 1145–1148.

85. S. D. Senturia, CAD for microelectromechanical systems, *Proc. Int. Conf. Solid-State Sensors Actuators (Transducers '95),* Stockholm, 1995.

86. N. R. Swart et al., AutoMM: Automatic generation of dynamic macromodels for MEMS devices, *Proc. IEEE Micro Electro Mech. Syst., Workshop (MEMS '98),* Heidelberg, 1998, pp. 178–183.

87. K. B. Albaugh, P. E. Cade, and D. H. Rasmussen, "Mechanisms of anodic bonding of silicon to pyrex glass," in *Int. Workshop on Solid-State Sensors and Actuators* (Hilton Head '88), p. 109.

Reading List

R. S. Muller et al., *Microsensors,* Piscataway, NJ: IEEE Press, 1991.

W. S. Trimmer (ed.), *Micromechanics and MEMS classic and seminal papers to 1990,* Piscataway, NJ: IEEE Press, 1997.

G. T. A. Kovacs, *Micromachined Transducers sourcebook,* New York: McGraw-Hill, 1998.

Stephen F. Bart
Microcosm Technologies

Michael W. Judy
Analog Devices

MICROMECHANICAL DEVICES AND FABRICATION.

See Micromachined devices and fabrication technologies.